Chapter 7
Numerical Simulation of Coir Geotextile Reinforced Soil Under Cyclic Loading

Jayan S. Vinod, Abdullah Al-Rawabdeh, Ana Heitor, and Beena K. Sarojiniamma

7.1 Introduction

Coir fibers are permeable natural fibers that are developed from the husk of the coconut. The coir fibers degrade very slowly compared to other natural fibers (e.g., jute), and the longevity of these fibers in the field is around 2–3 years (Dutta and Rao 2008). The limited use of non-renewable resources and the low cost of coir geotextiles have attracted attention toward using them as an alternative to synthetic geotextiles for infrastructure development (Sarsby 2007; Subaida et al. 2008, 2009; Chauhan et al. 2008; Vinod and Minu 2010; Hejazi et al. 2012; Balan 2017). In the recent past, many studies have been carried out on the bearing capacity of soil using synthetic polypropylene materials (Unnikrishnan et al. 2002; Bueno et al. 2005; Hufenus et al. 2006; Basudhar et al. 2008; Rawal and Sayeed 2013). Unnikrishnan et al. (2002) showed that the efficacy of placing reinforcement in soil is related to the stress transfer from the soil to the reinforcement. Basudhar et al. (2008) developed a linear elastic model using the finite element method on synthetic geotextile reinforcing sand under strip loading. A parametric study was conducted to investigate the geotextile's reinforcement depth. Many studies are reported on the bearing capacity of coir geotextile reinforced soil during monotonic loading (Noorzad and Mirmoradi 2010; Bhandari and Han 2010; Lal et al. 2017; Sridhar and Prathap Kumar 2018). Rashidian et al. (2018) studied the effect of the depth of

J. S. Vinod (✉) · A. Al-Rawabdeh
School of Civil Mining and Environmental Engineering, University of Wollongong, Wollongong, NSW 2522, Australia
e-mail: vinod@uow.edu.au

A. Heitor
School of Civil Engineering, University of Leeds, Leeds, UK

B. K. Sarojiniamma
Division of Civil Engineering, School of Engineering, Cochin University of Science and Technology, Kochi, Kerala, India

T. G. Sitharam et al. (eds.), *Latest Developments in Geotechnical Earthquake Engineering and Soil Dynamics*, Springer Transactions in Civil and Environmental Engineering, https://doi.org/10.1007/978-981-16-1468-2_7

placement of coir geotextiles and reported that the bearing capacity varies with the geotextile's position. In addition, the number of layers has an insignificant effect on the bearing capacity of soil. Kurian et al. (1997) presented a 3D nonlinear finite element model of a sand foundation reinforced with coir rope. A significant reduction in the settlement was observed for the coir reinforced foundation compared to the unreinforced model.

Performance under cyclic loading is considered to be crucial for the design of infrastructure for transport and seismic loading. Many studies reported the cyclic behavior of geosynthetic reinforced soil (Das and Shin 1994; Naeini and Gholampoor 2014; Sreedhar and Goud 2011). Raymond and Williams (1978) conducted a repeated triaxial test and indicated that the deformation under repeated loading is higher than the magnitude of deformation under static loading. Cunny and Sloan (1962) studied the dynamic loading effect on footing to establish a criterion for designing foundations under cyclic loading. Vesic et al. (1965) have concluded that the bearing capacity of footing under cyclic loading is less than the bearing capacity under static loading. Brumund and Leonards (1972) studied the behavior of circular footing on sand under dynamic loading and presented a linear relationship between footing settlement and peak acceleration. Al-Qadi et al. (2008) presented the efficiency of using geogrid in low-volume flexible pavements under dynamic loads. They showed that placing the geogrid between the subbase and subgrade layers gives the best performance for thin-layered base courses, while placing the geogrid at the depth of one-third of the base layer is the best for thick-based layers. Perkins et al. (2011) developed a two-dimensional model for geosynthetic reinforced unpaved roads to study the rutting deformation of flexible pavements. Sridher and Prathap Kumar (2018) investigated the behavior of coir geotextile reinforced sand under cyclic loading and concluded that placing the coir geotextile improves the sand's bearing capacity and reduces its settlement. However, only limited research studies focused on the cyclic behavior of coir geotextile reinforced soil (Sridhar and Prathap Kumar 2018).

The main objective of this research is to evaluate the mechanical behavior of coir geotextile reinforced soil during cyclic loading using a finite element method. The effect of different parameters influencing the performance of coir geotextile reinforced soil under cyclic loading is investigated and reported.

7.2 Numerical Model for Coir Geotextile Reinforced Soil Under Cyclic Loading

The finite element model for cyclic loading was created using Plaxis 2D. The soil bed has two soil layers: The first layer (layer I) is classified as (GW) crushed stone with high-quality material based on the unified soil classification system, and the second layer (layer II) is classified as (CH) clay with low-quality material. These two soils layers with different strengths were selected to understand the interaction

between various soils and coir geotextiles. The test tank model has dimensions of 800 mm length × 500 mm width. The model dimensions are similar to the laboratory experimental program reported by Subaida et al. (2009). Figure 7.1 shows the test conditions used for this study. The vertical load was applied on the left corner of the model by a 100-mm-diameter plate having a thickness of 25 mm. Only a half portion of the test bed was modeled considering the symmetry of the test bed. The hardening soil model with small strains (HSsmall) which is an advanced model designed by Schanz et al. (1999) has been considered for all soil layers. The material parameters used for the model were evaluated using laboratory tests reported by Subaida et al. (2009) and Sridhar and Prathap Kumar (2018). Table 7.1 presents the soil properties for layer I, layer II and sand soil for the hardening soil with small strains model (HSsmall).

The physical properties such as dry unit weight, saturated unit weight and Poisson's ratio (Bowles 1996) have been defined inclusive of strength parameters like lateral earth pressure, friction angle and dilatancy angles (Das et al. 2016) and the stiffness properties E_{oed}, E_{50} and Eur (Brinkgreve et al. 2014). In this study, the soil layers were considered to be dry.

The coir geotextile was modeled as a linear elastic plate element and assigned a bending stiffness (EI) value of 0.15E−9 kNm^2/m, and the elastic stiffness (EA) is 500 kN/m. The lateral deformation is restricted on the left and right boundary walls, and both lateral and vertical deformations are restricted for the bottom boundary of the model. The coir geotextile in the model represents woven coir geotextile with 1286.56 g/m^2 mass/unit area, 20.7 and 36 kN/m weft and warp tensile strength, respectively.

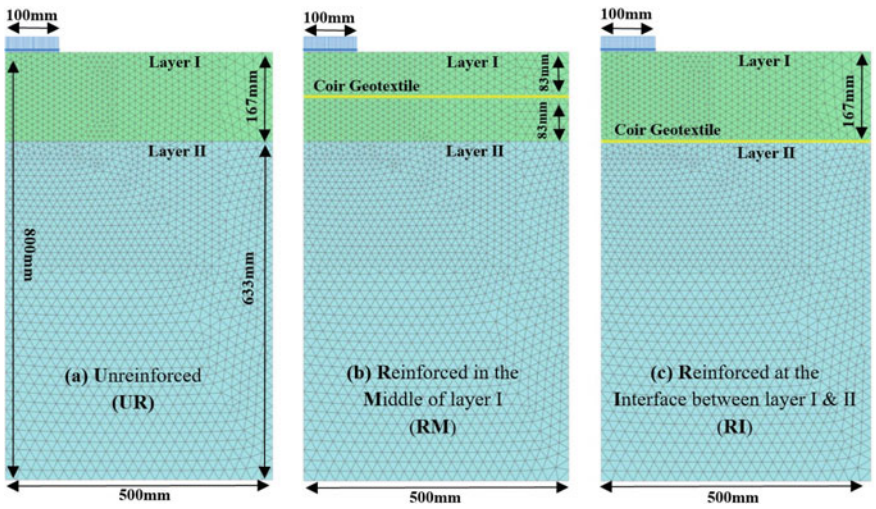

Fig. 7.1 Test models; **a** unreinforced soil (UR), **b** reinforcement in the middle of layer (I) and **c** reinforcement at the interface between layers (I) and (II)

Table 7.1 Layer I, layer II and sand soil properties (hardening soil model with small strains)

General, stiffness and strength parameters	Symbol	Unit	Value		
			Layer I	Layer II	Sand[a]
Dry unit weight	γ_d	kN/m^3	18	12	17.4
Saturated unit weight	γ_{sat}	kN/m^3	21	16.95	19.96
Void ratio	e	–	0.46	1.02	0.5
Tangent stiffness for primary oedometer loading	E_{oed}	kN/m^2	10,000	350	75,00
Secant stiffness in standard drained triaxial test	E_{50}	kN/m^2	12,500	700	10,000
Unloading/reloading stiffness	Eur	kN/m^2	45,000	2100	30,000
Power for stress-level dependency of stiffness	m	–	0.5	0.5	0.5125
Shear strain level, where the secant shear modulus reduced to 70% of G_0	$\gamma_{0.7}$	–	2×10^{-4}	0.1×10^{-3}	0.1×10^{-3}
Initial shear modulus	G_0	kN/m^2	140,000	8400	120,000
Coefficient of earth pressure	K_0	–	0.253	–	0.293
Friction angle	ϕ	0	48.3	–	45
Dilatancy angle	ψ	0	19	–	15
Cohesion	C	kN/m^2	–	19.5	–

[a]The sand soil layer used in the dynamic load validation

A typical sinusoidal cyclic loading with variant frequency and cyclic stresses (σ_c) is used to study the cyclic behavior of coir geotextile reinforced soil. In this investigation, number of cycles (N), cyclic stress amplitudes (σ_c = 50, 100, 150 kPa) and frequency (f = 0.5, 1, 1.5 Hz) were varied during cyclic loading.

7.3 Results and Discussion

7.3.1 Calibration of FE Model

Calibration of the finite element model for cyclic loading was carried out on a model having dimensions of 500 mm length and width (See inset of Fig. 7.2). The cyclic load was applied through a 50 mm circular footing (Sridhar and Prathap Kumar 2018). Figure 7.2 shows the settlement of sand with the number of cycles during cyclic loading. The model was subjected to a cyclic stress of 100 kPa and f = 0.5 Hz. It is evident from Fig. 7.2 that the numerical model captures the settlement of sand during cyclic loading similar to the laboratory experiment reported by Sridhar and Prathap Kumar (2018). The sand properties are found in Table 7.1 and the model geometry in Fig. 7.2. The footing settlement increases with the increase of the number of cycles, and the significant increase in the settlement of footing was observed for $N > 2000$.

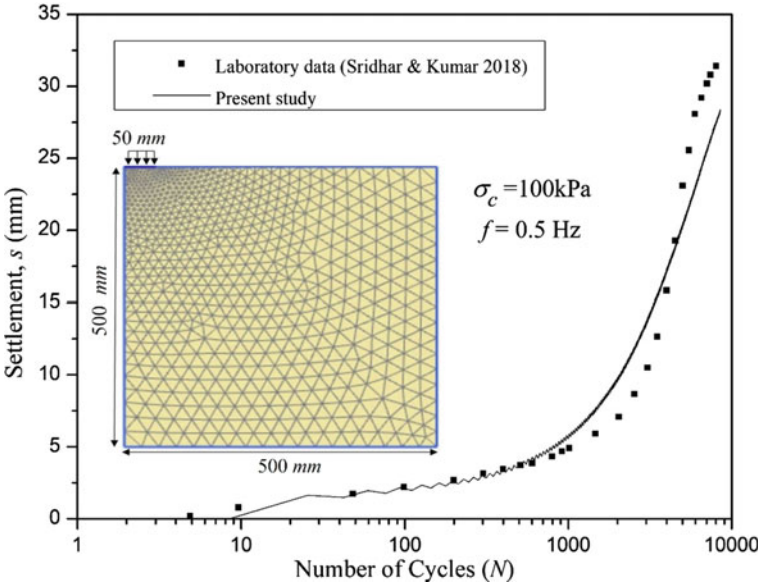

Fig. 7.2 Calibration of FEM model for cyclic loading

7.3.2 *Behavior of Coir Geotextile Reinforced Soil During Cyclic Loading*

Figure 7.3 shows the variation of *s/B* with *N* for UR, RI and RM for σ_c= 150 kPa and f = 0.5 Hz, where *s/B* is settlement over plate width ratio. It is evident from Fig. 7.3 that the inclusion of coir geotextiles reduces the *s/B* of soil during cyclic loading, and it is interesting to note that the initial stiffness increases with the inclusion of coir geotextiles. The coir geotextiles placed in the middle of layer I (RM) exhibits lower settlement compared to RI. For a particular value of *N* (say *N* = 10,000), the UR shows an *s/B* of 23% compared with 14% and 19% for RM and RI, respectively.

7.3.3 *Effect of Cyclic Stress on the Settlement of Coir Geotextile Reinforced Soil*

Figure 7.4 shows the effect of cyclic stress on the settlement behavior of UR, RI and RM. As expected, the settlement increases with the increase in cyclic stress. At 10,000 cycles, *s/B* increased from 5.5 to 24% when the cyclic stress increased from 50 to 150 kPa for UR. For RM, *s/B* decreased to 15.6% at 150 kPa cyclic stress and 3.4% at 50 kPa cyclic stress. For RI, s*/B* decreased to 20.1% at 150 kPa and 4.2%

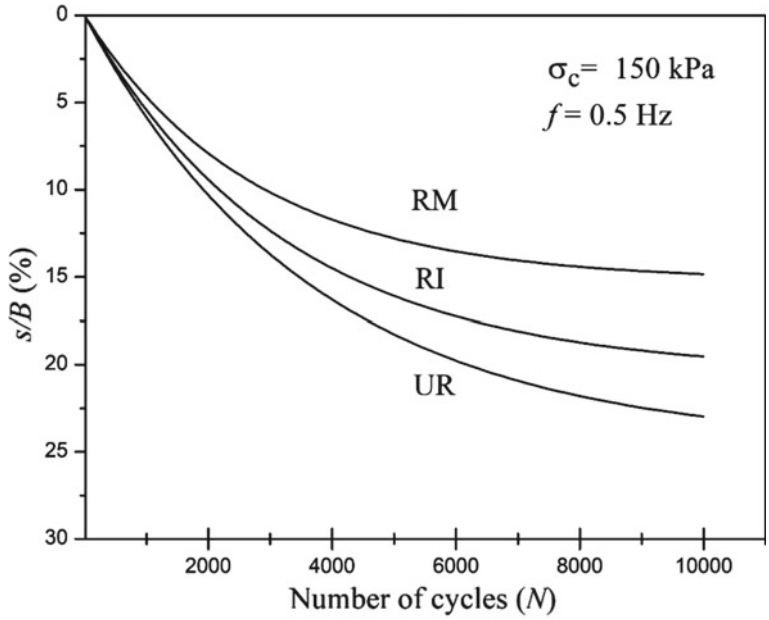

Fig. 7.3 Number of cycles—s/B relationship of unreinforced and reinforced soil with coir geotextiles

at 50 kPa. The maximum performance reduction in settlement was observed when the geotextile is placed in the middle of layer I (RM). The decrease in the footing settlement due to the placement of coir geotextiles at RI and RM for σ_c= 150 kPa was 16.3% and 35%, respectively. Nevertheless, for σ_c= 100 kPa, there is a 27.8 and 37.5% reduction in settlement for RI and RM, respectively. Table 7.2 summarizes the footing settlement under different σ_c for UR, RI and RM.

Figure 7.4 also shows the relationship between *s/B* and *N* for different frequencies (*f*) of cyclic loading. It is evident from Fig. 7.4 that the *s/B* increases with *f* irrespective of the location of coir geotextiles. In fact, for UR *s/B* increases from 14.3% to 48.3% when *f* increases from 0.5 to 1.5 Hz for *N* = 10,000. For RI, *s/B* decreased to 10.4% at 0.5 Hz and 46.2% at 1.5 Hz, and for RM, *s/B* decreased to 9.6% at 0.5 Hz and 33.3% at 1.5 Hz. The optimum performance of coir geotextiles in reducing settlement was observed for RM for the σ_c and *f* considered for this study.

The potential of the geotextile in controlling the settlements of the footing can be clearly seen in Table 7.2. Increasing the cyclic stress increases the footing settlement, while incorporating coir geotextiles at (RI) and in (RM) enhances soil performance and reduces settlement. The footing experienced a 23.6 and 38.2% reduction in settlement for RI and RM under 50 kPa and 27.8% and 37.5%

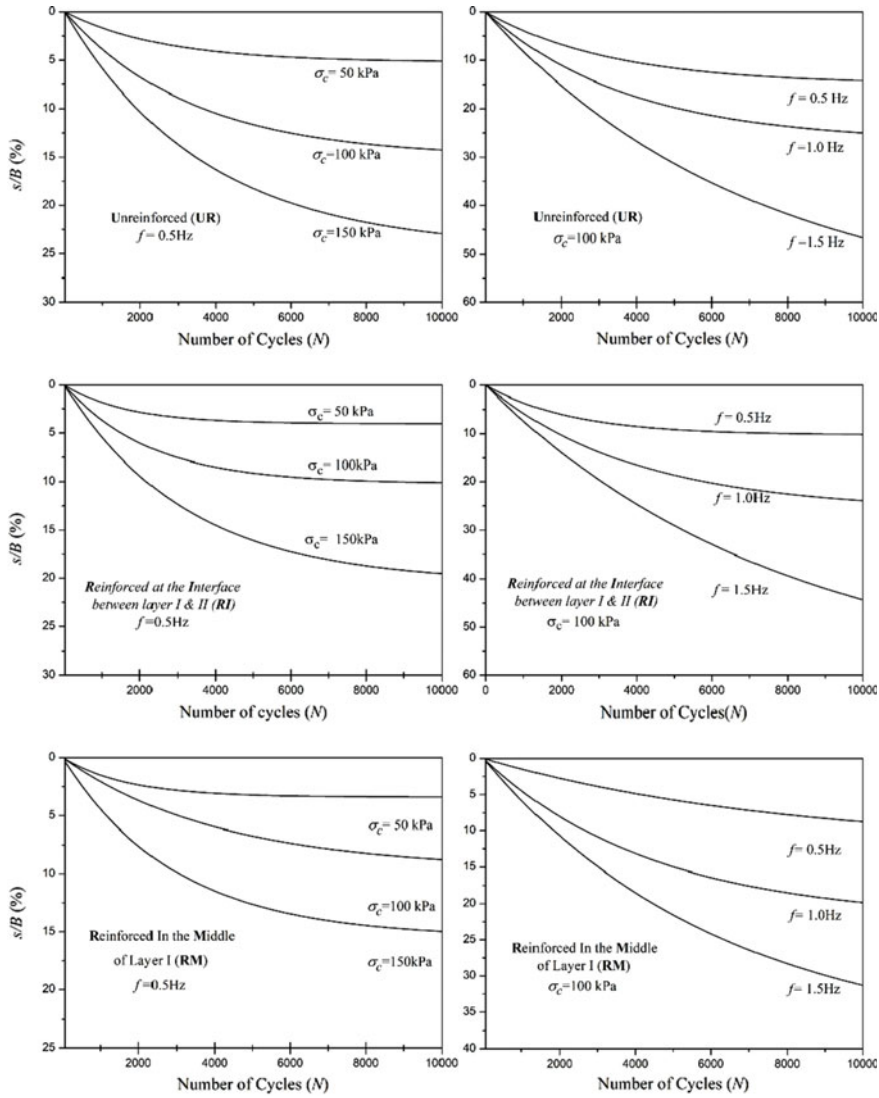

(A) Effect of cyclic stress (σ_c) (B) Effect of frequency (f)

Fig. 7.4 Number of cycles—s/B curve; **a** various cyclic stresses and **b** various frequencies on unreinforced and reinforced soils

respectively, under 100 kPa cyclic stresses. While under 150 kPa cyclic stress, the coir geotextile at RI shows a 16.3% reduction in settlement and a 35% for RM. This shows that placing the coir geotextile in the middle of layer I results in an optimum performance of the geotextile in controlling settlements.

Table 7.2 Effect of cyclic stress on geotextile performance

Test	Amplitude (kPa)	Number of cycles (*N*)	*s/B* (%)	% Reduction in settlement (%)
	50		5.5	–
UR	100	10,000	14.4	–
	150		24	–
	50		4.2	23.6
RI	100	10,000	10.4	27.8
	150		20.1	16.3
	50		3.4	38.2
RM	100	10,000	9	37.5
	150		15.6	35

Table 7.3 Effect of frequency on geotextile performance

Test	Frequency (Hz)	Number of cycles (*N*)	*s/B* (%)	% Reduction in settlement (%)
UR	0.5		14.3	–
	1	10,000	26.4	–
	1.5		48.3	–
RI	0.5		10.4	27.3
	1	10,000	25.6	3
	1.5		46.2	4.3
RM	0.5		9.6	32.9
	1	10,000	21	20.5
	1.5		33.3	31.1

Table 7.3 summarizes the footing settlement under different f for UR, RI and RM. The ability of the geotextile to reduce the settlement of the footing can clearly be recognized, and the optimum performance occurred when the geotextile is placed in the middle of layer I (RM). The inclusion of a coir geotextile at RI and in RM enhanced the performance of soil and reduced settlement. For $f = 0.5$ Hz, a 27.3% and 32.9% reduction in *s/B* was observed for RI and RM, respectively. For $f = 1$ Hz, percentage reduction in *s/B* is 3% and 20.5% and for $f = 1.5$ Hz percentage reduction in *s/B* is 4.3% and 31.1% for RI and RM, respectively. These reductions in settlement indicate that placing the coir geotextile at RM has shown higher performance in terms of reducing settlement for the σ_c and f considered for this study.

7.3.4 Spatial Distribution of Stresses on Soil and Reinforcement During Cyclic Loading

Figure 7.5 shows the spatial stress distribution during cyclic loading for UR, RM and RI. The peak stress were captured when the assembly reaches a settlement of 40 mm. It is evident from Fig. 7.5 that peak stress for UR is 51.61 kN/m^2. However, for RM and RI the peak stress reaches 91.56 and 89.58 kN/m^2 respectively. The peak stress increases with the inclusion of coir geotextiles. The increase in the peak stress is mainly due to the additional axial tensile forces developed in the coir geotextile and has shown higher due to higher interface friction angle between soil and coir geotextiles.

Figure 7.6 shows the axial tensile force that developed in the geotextiles for RI and RM at N = 10,000 cycles. The maximum axial force for RM is 1.09 kN/m and for RI is 0.24 kN/m. The axial force observed in the coir geotextile for RM is about four times compared to RI. The frictional interaction between the coir geotextile and the soil generates interface shear stress in the coir geotextile. The axial tensile force developed in the coir geotextile is due to that interaction between the soil and the reinforcement during cyclic loading. The maximum axial force for RM generated at the middle of the footing decreases along the width of the footing. However, for RI, the axial force is found to distribute along the width of the footing. Moreover, a small amount of negative axial force is also seen to develop along the

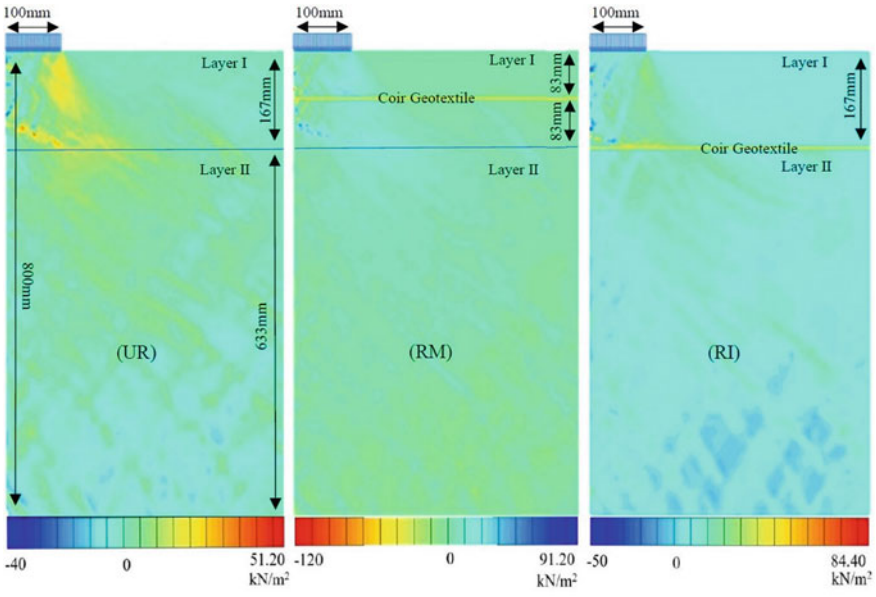

Fig. 7.5 Spatial stress distribution in unreinforced and reinforced soils with coir geotextiles under cyclic loading

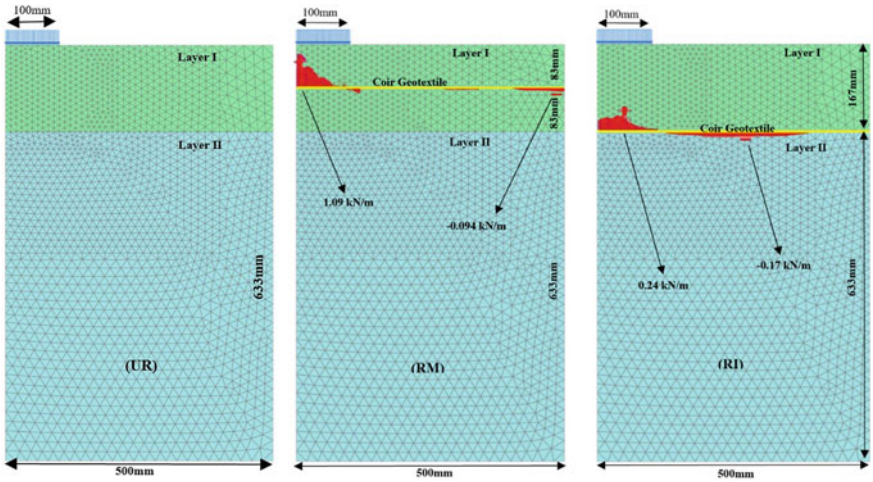

Fig. 7.6 Axial force developed in coir geotextile during cyclic loading

reinforcement for the case of RM. The negative value represents the generated shear force in coir geotextiles and soil in the direction opposite to the soil movement. The interface shear stress is mainly due to frictional interaction between the coir geotextile's surface and soil particles, thus aiding the geotextile to generate axial forces during cyclic loading as presented in Fig. 7.6. This observation is consistent with the experimental study, reported by Nguyen et al. (2013). Nguyen et al. (2013) report on the generation of shear stress in coir geotextile and soil in the transverse direction of the soil movement.

7.4 Conclusions

The numerical model captures the behavior of soil in the same way as the laboratory experiments reported by Sridhar and Prathap Kumar (2018). Coir geotextiles were installed at the interface between layers I and II (RI), and in the middle of layer I (RM). The inclusion of coir geotextiles in the middle of layer I yielded their best performance during cyclic loading. The inclusion of coir geotextiles in soil during cyclic loading reduces settlement and thus improves the performance of soil. The cyclic stress and frequency have a significant influence on the settlement of footing. The *s/B* was found to be increasing with the increase in the cyclic loads and frequency. Placing the coir geotextile in the middle of layer I (RM) has shown the best performance in term of the load carrying capacity of soil and may be due to the development of the interface shear stress in the coir geotextile. The interface friction

between the soil and the coir geotextile generates an interface shear stress, and an axial force in the geotextile and consequently increases the load carrying capacity and reducing the settlement.

Acknowledgements The authors gratefully acknowledge the support of the Coir Board (Govt of India), University of Wollongong and Cochin University of Science and Technology (CUSAT), through EIS Partnership grant in carrying out this research. The first author also thanks the support from the Australian Academy of Science for funding Australia-India EMCR fellowship for this research project.

References

Al-Qadi IL, Dessouky SH, Kwon J, Tutumluer E (2008) Geogrid in flexible pavements: validated mechanism. Transp Res Rec 2045(1):102–109. https://doi.org/10.3141/2045-12

Balan K (2017) Coir geotextiles in infrastructure projects. Indian J Geosynthetics Ground Improv 6(2):8–16

Basudhar P, Dixit P, Gharpure A, Deb K (2008) Finite element analysis of geotextile- reinforced sand-bed subjected to strip loading. Geotext Geomembr 26(1):91–99. https://doi.org/10.1016/j.geotexmem.2007.04.002

Bhandari A, Han J (2010) Investigation of geotextile–soil interaction under a cyclic vertical load using the discrete element method. Geotext Geomembr 28(1):33–43. https://doi.org/10.1016/j.geotexmem.2009.09.005

Bowles L (1996) Foundation analysis and design. McGraw-hill, New York, pp 32–90

Brinkgreve R, Kumarswamy S, Swolfs W, Waterman D, Chesaru A, Bonnier P (2014) Plaxis 2014. Plaxis BV, The Netherlands

Brumund WF, Leonards GA (1972) Subsidence of sand due to surface vibration. J Soil Mech Found 98(1):27–42

Bueno BS, Benjamim CVS, Zornberg JG (2005) Field performance of a full-scale retaining wall reinforced with non-woven geotextiles. Slopes and retaining structures under seismic and static conditions. ASCE 1–9. https://doi.org/10.1061/40787(166)1

Chauhan MS, Mittal S, Mohanty B (2008) Performance evaluation of silty sand sub- grade reinforced with fly ash and fibre. Geotext Geomembr 26(5):429–435. https://doi.org/10.1016/j.geotexmem.2008.02.001

Cunny R, Sloan R (1962) Dynamic loading machine and results of preliminary small-scale footing tests. Symp Soil Dyn. https://doi.org/10.1520/STP44378S

Das B, Shin E (1994) Strip foundation on geogrid-reinforced clay: behavior under cyclic loading. Geotext Geomembr 13(10):657–667. https://doi.org/10.1016/0266-1144(94)90066-3

Das B, Sobhan K, Das B (2016) Principles of geotechnical engineering, 8th edn, SI edn. Cengage Learning, Boston

Dutta R, Rao GV (2008) Potential of coir based products as soil reinforcement. Int J Earth Sci Eng 1(2):71–79

Hejazi SM, Sheikhzadeh M, Abtahi SM, Zadhoush A (2012) A simple review of soil reinforcement by using natural and synthetic fibers. Constr Build Mater 30:100–116. https://doi.org/10.1016/j.conbuildmat.2011.11.045

Hufenus R, Rueegger R, Banjac R, Mayor P, Springman SM, Brönnimann R (2006) Full-scale field tests on geosynthetic reinforced unpaved roads on soft subgrade. Geotext Geomembr 24(1):21–37. https://doi.org/10.1016/j.geotexmem.2005.06.002

Kurian NP, Beena K, Kumar RK (1997) Settlement of reinforced sand in foundations. J Geotech Geoenviron Eng 123(9):818–827. https://doi.org/10.1061/(ASCE)1090-0241(1997)123:9(818)

Lal D, Sankar N, Chandrakaran S (2017) Effect of reinforcement form on the behaviour of coir geotextile reinforced sand beds. Soils Found 57(2):227–236. https://doi.org/10.1016/j.sandf.2016.12.001

Naeini S, Gholampoor N (2014) Cyclic behaviour of dry silty sand reinforced with a geotextile. Geotext Geomembr 24(6):611–619. https://doi.org/10.1016/j.geotexmem.2014.10.003

Nguyen MD, Yang KH, Lee SH, Wu CS, Tsai MH (2013) Behavior of nonwoven-geotextile-reinforced sand and mobilization of reinforcement strain under triaxial compression. Geosynthetics Int 20(3):207–225. https://doi.org/10.1680/gein.13.00012

Noorzad R, Mirmoradi S (2010) Laboratory evaluation of the behavior of a geotextile reinforced clay. Geotext Geomembr 28(4):386–392. https://doi.org/10.1016/j.geotexmem.2009.12.002

Perkins S, Christopher B, Lacina B, Klompmaker J (2011) Mechanistic-empirical modeling of geosynthetic-reinforced unpaved roads. Int J Geomech 12(4):370–380. https://doi.org/10.1061/(ASCE)GM.1943-5622.0000184

Rashidian V, Naeini SA, Mirzakhanlari M (2018) Laboratory testing and numerical modelling on bearing capacity of geotextile-reinforced granular soils. Int J Geotech Eng 12(3):241–251. https://doi.org/10.1080/19386362.2016.1269042

Rawal A, Sayeed M (2013) Mechanical properties and damage analysis of jute/poly- propylene hybrid nonwoven geotextiles. Geotext Geomembr 37:54–60. https://doi.org/10.1016/j.geotexmem.2013.02.003

Raymond GP, Williams DR (1978) Repeated load triaxial tests on dolomite ballast. J Geotech Geoenviron Eng 104(7)

Sarsby RW (2007) Use of 'Limited Life Geotextiles' (LLGs) for basal reinforcement of embankments built on soft clay. Geotext Geomembr 25(4–5):302–310. https://doi.org/10.1016/j.geotexmem.2007.02.010

Schanz T, Vermeer PA, Bonnier PG (1999) The hardening soil model: formulation and verification. In: Brinkgreve RBJ (ed) Beyond 2000 in computation geotechniques. Rotterdam, the Netherlands, pp 281–290

Sreedhar M, Goud APK (2011) Behaviour of geosynthetic reinforced sand bed under cyclic load. In: Proceedings of Indian geotechnical conference, Kochi, India, pp 15–17

Sridhar R, Prathap Kumar MT (2018) Effect of number of layers on coir geotextile reinforced sand under cyclic loading. Geo-Eng 9(1):11. https://doi.org/10.1186/s40703-018-0078-y

Subaida E, Chandrakaran S, Sankar N (2008) Experimental investigations on tensile and pullout behaviour of woven coir geotextiles. Geotext Geomembr 26(5):384–392. https://doi.org/10.1016/j.geotexmem.2008.02.005

Subaida E, Chandrakaran S, Sankar N (2009) Laboratory performance of unpaved roads reinforced with woven coir geotextiles. Geotext Geomembr 27(3):204–210. https://doi.org/10.1016/j.geotexmem.2008.11.009

Unnikrishnan N, Rajagopal K, Krishnaswamy N (2002) Behaviour of reinforced clay under monotonic and cyclic loading. Geotext Geomembr 20(2):117–133. https://doi.org/10.1016/S0266-1144(02)00003-1

Vesic A, Banks D, Woodard J (1965) An experimental study of dynamic bearing capacity of footings on sand. In: Proceedings of VI international conference on soil mechanics and foundation engineerin, Canada, Montreal, (2), pp 209–213

Vinod P, Minu M (2010) Use of coir geotextiles in unpaved road construction. Geosynthetics Int 17(4):220–227. https://doi.org/10.1680/gein.2010.17.4.220